A study into the impact of interface roughness development on mechanical degradation of oxides formed on zirconium alloys

P. Platt [a,*], S. Wedge [b], P. Frankel [a], M. Gass [b], R. Howells [b], M. Preuss [a]

[a] University of Manchester, School of Materials, Materials Performance Centre, Manchester M13 9PL, UK
[b] AMEC, Walton House, Faraday Street, Birchwood Park, Risley, Warrington WA3 6GA, UK

ARTICLE INFO

ABSTRACT

As a cladding material used to encapsulate nuclear fuel pellets, zirconium alloys are the primary barrier separating the fuel and a pressurised steam or lithiated water environment. Degradation mechanisms such as oxidation can be the limiting factor in the life-time of the fuel assembly. Key to controlling oxidation, and therefore allowing increased burn-up of fuel, is the development of a mechanistic understanding of the corrosion process. In an autoclave, the oxidation kinetics for zirconium alloys are typically cyclical, with periods of accelerated kinetics being observed in steps of $\sim$2 μm oxide growth. These periods of accelerated oxidation are immediately preceded by the development of a layer of lateral cracks near the metal-oxide interface, which may be associated with the development of interface roughness. The present work uses scanning electron microscopy to carry out a statistical analysis of changes in the metal-oxide interface roughness between three different alloys at different stages of autoclave oxidation. The first two alloys are Zircaloy-4 and ZIRLO™ for which analysis is carried out at stages before, during and after first transition. The third alloy is an experimental low tin alloy, which under the same oxidation conditions and during the same time period does not appear to go through transition. Assessment of the metal-oxide interface roughness is primarily carried out based on the root mean square of the interface slope known as the R_{dq} parameter. Results show clear trends with relation to transition points in the corrosion kinetics. Discussion is given to how this relates to the existing mechanistic understanding of the corrosion process, and the components required for possible future modelling approaches.

1. Introduction

Zirconium alloys are used as cladding to encapsulate fuel pellets in pressurised and boiling water nuclear reactors. Research into oxidation of these alloys has been significant since the introduction of the material. However, the microstructure and electro-chemical processes during oxidation are complex and many questions still remain unanswered. One such issue is the formation of lateral cracks near the metal-oxide interface. Small cracks have been seen to form continuously during oxidation, with large scale networks of lateral cracks forming cyclically every $\sim$2 μm of oxide growth. These networks of cracks can be correlated with acceleration in the corrosion kinetics [1–7]. These lateral cracks might enable the link up of nano pores along grain boundaries perpendicular to the metal/oxide interface as reported in [8,9]. Experiments using Synchrotron X-Ray Diffraction (S-XRD) by both Polatidis et al. and Petigny et al., have separately shown that oxides formed on Zirca-

loy-4 are composed of monoclinic and stabilised tetragonal phases, with an $\sim$7% reduction in the tetragonal phase fraction from 1 to 3 μm oxide growth [4,10]. One theory is that the lateral cracks may destabilise the tetragonal phase close to the metal-oxide interface. The phase transformation has an $\sim$6% expansion associated with it, which could lead to fracture perpendicular to the metal-oxide interface, thereby generating fast ingress routes for oxygen containing species [11,12].

Work by Bossis et al. [2], Ly et al. [5], and Ni et al. [13], have all indicated an increase in interfacial roughness with oxidation of zirconium alloys. However, connecting this with transition in the corrosion kinetics can be more problematic. When considering the interface undulations to be similar to a sinusoidal wave, Bossis et al. have said that the interface develops a fairly consistent wavelength of $\sim$1 μm, and that the amplitude increases progressively up to transition in the corrosion kinetics. The rapid oxidation reduces the amplitude, which would in theory allow the process to cycle [2,14]. Ni et al. used FIB slice and view to characterise the development of interface roughness and lateral crack formation in 3D [13].

The root mean square of the interface roughness appears to increase up to transition and then drop sharply in line with the work by Bossis et al. [2]. Ly et al. could not identify a typical wavelength using Fast Fourier Transform, and although interface roughness increases with oxidation no clear link to transition could be identified [5].

There are two probable causes of interface roughness formation. The first is that this is a deformation mechanism designed to relieve some of the stresses induced by the expansion as the metal transforms into oxide [15–17]. Indeed finite element analysis predicts the plastic deformation of the metal substrate in the presence of interface roughness [18]. TEM carried out by Tejland et al. has seen evidence of dislocation clusters and sub-grain formations. The paper details why this is most likely to be a result of localised deformation due to interface roughness development [19]. The second possibility is that interface roughness forms due to variation in oxygen diffusion rates through the oxide layer [17,20]. Oxides formed on zirconium alloys are composed of monoclinic and tetragonal phases, both of which demonstrate high levels of compressive stress [4]. This has the potential to impact oxygen diffusion through the lattice and along grain boundaries. High resolution SIMS analysis of ^{18}O doping oxidation tests indicated that the lateral cracks might locally impede oxygen diffusion, thereby contributing to interface roughness development [21].

Lateral cracks have been seen to form preferentially above peaks in the interface roughness, or delays in the advancing oxidation front [2,13,14,22]. Finite element analysis has indicated that the expansion of newly formed oxide above interface peaks should result in a strong tensile stress perpendicular to the metal-oxide interface [18]. These tensile stresses could potentially cause the localised fracture of the oxide layer, or separation of the metal-oxide interface. Isolated cracks have been observed to form continuously during the oxidation process [2,5,13]. Although they have been seen to initiate above emerging SPPs (second phase particles) above a certain size, many lateral cracks form in the absence of SPPs meaning another mechanism must be primarily responsible [5]. There is some disagreement relating crack formation with transition in the corrosion kinetics. Bossis et al. and Ly et al. have both said that networks of lateral cracks form at transition (~2 μm oxide growth), i.e. before the acceleration in the corrosion kinetics [2,5]. The work by Ni et al. states that the crack volume fraction increases linearly with oxide thickness, and therefore the layers of lateral cracks, that are present at ~2 μm intervals, form during the accelerated oxidation phase rather than immediately before.

Other materials which form strongly compressed oxide layers during high temperature oxidation have been seen to form interface roughness, and subsequently separation of the interface or fracture of the oxide [16,17,23,24]. A common approach has been the application of fracture mechanics to develop energy models of the oxidation process. The basic theory being that a compressed oxide layer contains stored elastic energy which can be relaxed by increasing the interfacial area [16,23]. However, this increases the interfacial energy and leads to strain hardening of the substrate. Therefore, at some stage it becomes energetically favourable to induce spallation of the oxide layer [15,20]. Research of this type is significant and worth considering when analysing oxidation of zirconium alloys.

The aim of the work presented here is to analyse the development of roughness at the metal-oxide interface for a range of zirconium alloys and connect this with the transition points and associated acceleration in the corrosion kinetics. This will be used to enhance the current mechanistic understanding of zirconium alloy corrosion.

2. Experimental

The materials that have been assessed are Zircaloy-4 (sheet), ZIRLO™ (tube), and A-0%Sn (tube). The samples were prepared by pickling using a dilute hydrofluoric acid solution, followed by autoclave testing in 360 °C primary water at ~18 MPa by EDF-R&D at Moret-sur-Loing, France. Further experimental details can be found in [4] and [25]. The weight gain measurements for Zircaloy-4 have been converted into average oxide thicknesses and can be found in Fig. 1a. The Zircaloy-4 sheet exhibits transition and acceleration in the oxidation kinetics somewhere between 160 and 200 days. Assessing the alloy chemistries shown in Table 1 it can be seen that the A-0%Sn tube material is very similar to that of the ZIRLO™ tube but with <0.0% Sn. This makes the direct comparison of the oxidation behaviour of these materials very valuable. The weight gain measurements for ZIRLO™ and A-0%Sn can be seen in Fig. 1b. The ZIRLO™ appears to go through transition between 140 and 160 days, whereas the A-0%Sn does not go through transition during the period analysed.

Samples from these materials were mounted in cross-section, ground, and polished with a colloidal silica OPS (oxide polishing solution). Analysis of the metal-oxide interface was carried out using an FEI Quanta 200 Scanning Electron Microscope (SEM) in backscattered electron mode. The samples that have been mounted and analysed have been circled in Fig. 1a and b. For the Zircaloy-4 material 7 samples were analysed, with ~100 images taken at random across a distance of ~30 mm per sample. For the Zircaloy-4 material the surface of the oxide layer remained largely intact after sample preparation, allowing analysis of the oxide thickness and comparison of interface roughness with oxide thickness for each image. 5 samples of the ZIRLO™ and A-0%Sn material were analysed, with ~30 images taken at random across a distance of ~10 mm per sample. For the ZIRLO™ and A-0%Sn materials, small amounts of damage to the surface of the oxide layer during sample preparation made analysis of the oxide thickness via SEM
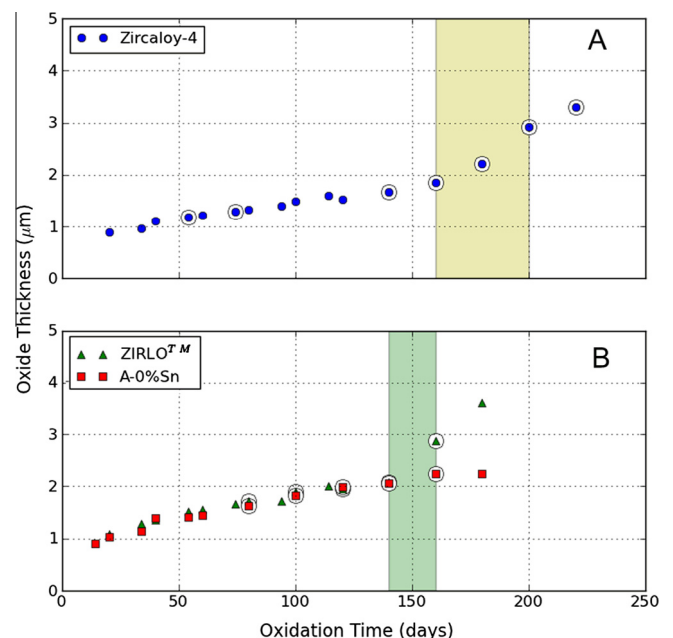

Fig. 1. The oxidation kinetics for Zircaloy-4 sheet material (A), and ZIRLO™ & A-0%Sn tube materials (B), in 360 °C primary water, with the light yellow and green bars representing the interval in time when transition appears to have occurred for the Zircaloy-4 and ZIRLO™ materials respectively. (For interpretation of the references to colour in this figure legend, the reader is referred to the web version of this article.)

Table 1
Summary of zirconium alloys analysed.

Alloy	Heat treatment	Geometry	Alloying elements (wt.%)			
			Sn	Fe	Cr	Nb
Zircaloy-4	Recrystallised	Sheet	1.24	0.17	0.1	<0.01
ZIRLO™	Recrystallised	Tube	0.92	0.09	<0.01	0.91
A-0%Sn	Recrystallised	Tube	<0.01	0.1	<0.01	1.0
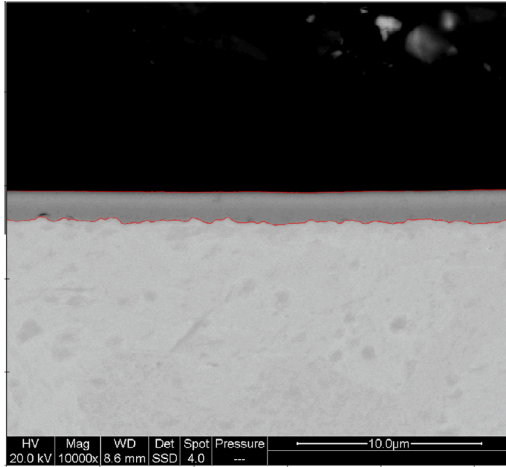
Fig. 2. An example of the image analysis used to define the metal-oxide interface and oxide surface.

impossible. For all materials each image was taken at 10,000× magnification covering ~28 µm of interface. Across the three materials 17 samples were analysed: 7 for Zircaloy-4, 5 for ZIRLO™, and 5 for A-0%Sn, totalling ~1000 images in all. A small number of representative example images were taken at 16,000× magnification and are presented later in the paper.

Image analysis was carried out using a script purposely developed for SEM cross-section analysis of zirconium alloys at AMEC, Risley, UK using the Enthought Python Distribution package. This script allows the automated extraction of the metal-oxide interface as a series of X–Y coordinates based on the difference in contrast between the pixels of each region. Fig. 2 shows an example of the image analysis script used to define the metal-oxide interface. All data analysis has been carried out using the Enthought Python Distribution package. As a result of this image analysis process the raw data for the interface is pixellated, introducing very fine scale noise into the data. Data smoothing was carried out on the extracted interface using a spline method to remove the effect of the pixellation (Fig. 3). The spline fitting has a modifiable

parameter, which changes the sensitivity to small scale variations in the roughness. If this parameter is set very low then the function attempts to fit the spline exactly, thereby including the pixellation noise. A parameterisation study was carried out to identify the lowest value for this parameter where a further increase did not result in a noticeable change in the roughness values and is therefore considered to have removed the pixellation noise.

3. Results & discussion

3.1. Oxide thickness – Zircaloy-4

The thickness of oxides formed on zirconium alloys are typically calculated via the weight gain after oxidation. This calculation is shown in Eq. (1) [26];

$$t = \frac{W}{f_O D} \tag{1}$$

where W is the weight gain in mg per dm^2, f_O is the weight percentage of oxygen in the zirconia phase and D is the density of the monoclinic phase. This results in an equivalence of 15 mg/dm^2 weight gain giving an oxide thickness of 1 µm. For the Zircaloy-4 material the oxide was found to be largely intact after the samples had been mounted and polished. As such, the image analysis process was able to fit a profile to both the metal-oxide interface and the oxide surface for all images taken of the Zircaloy-4 material (Fig. 2). By subtracting the X–Y coordinates for the metal-oxide interface from those of the oxide surface, it is possible to define the average oxide thickness for each image. A comparison of the oxide thickness defined by weight gain and by SEM imaging is shown in Fig. 4. Each SEM data point represents the median of 100 images, with the scatter bars being defined by the upper and lower quartile. Although the trends are the same for both techniques, using SEM appears to define a thicker oxide layer for almost every sample when compared with the weight gain calculation.

The weight gain calculations are based on the idea that the oxide is stoichiometric, compact and defect free. Assessment of these oxides has shown that this is not the case. As shown in Figs. 5–7, oxides that form on zirconium alloys in autoclaves contain pores, cracks and un-oxidised SPPs. It has also been indicated that the oxide that forms may well be sub-stoichiometric and oxygen deficient [27–29]. This will give a thicker, less dense and non-homogenous oxide layer compared with that, which is predicted by calculation of the weight gain.

3.2. Qualitative assessment of defects – Zircaloy-4

Fig. 5a–c shows example images taken of the Zircaloy-4 material after 54 days, 160 days and 200 days. This represents time
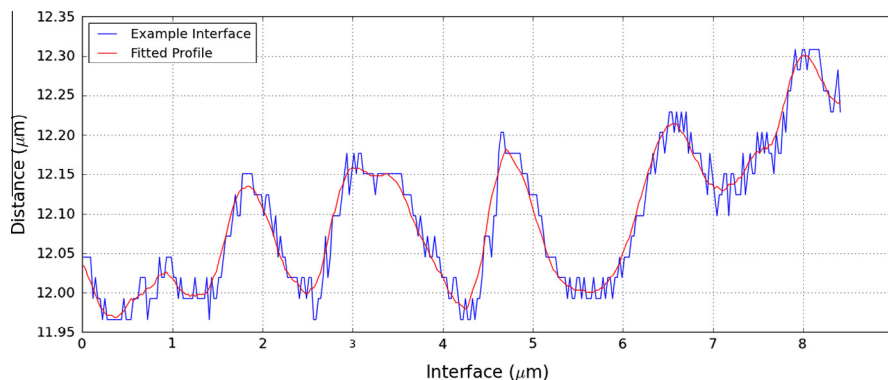

Fig. 3. An example of data smoothing using a spline method to remove the effect of pixellation.
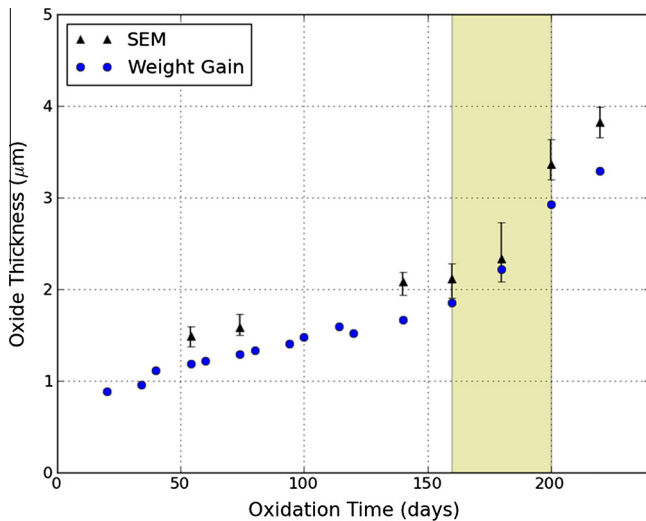
Fig. 4. Comparison of changes in the oxide thickness over time defined by the weight gain calculation and SEM imaging for the Zircaloy-4 material.
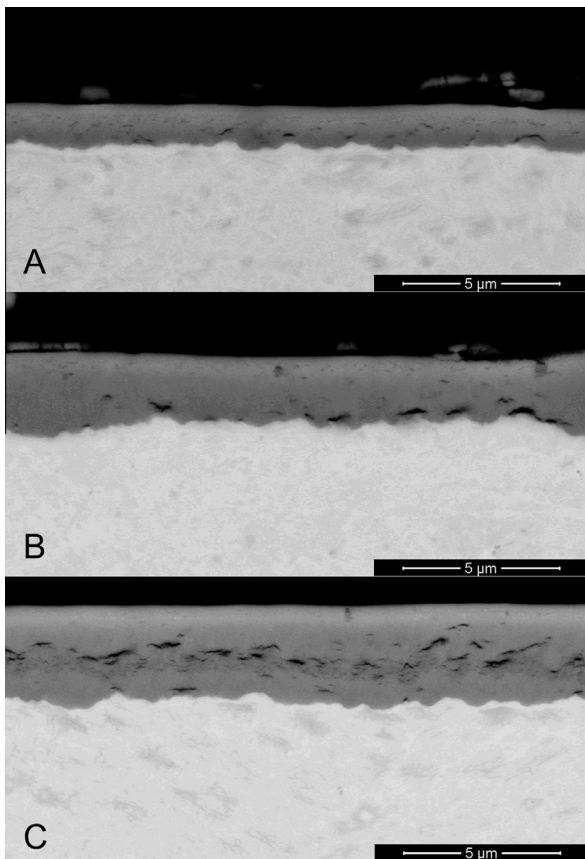

Fig. 5. SEM cross section images (16000× mag.) of Zircaloy-4 samples after 54 days, 160 days and 200 days oxidation respectively.

intervals far before transition, just before or at transition, and after transition has occurred as defined by the weight gain measurements. These images were taken at 16,000× magnification and are designed to be representative examples of the oxide and oxide-metal interface. Fig. 5a shows that any cracks at the metal-oxide interface are sparse and appear isolated. In contrast, 160 days oxidation is just before transition for Zircaloy-4 and, accordingly, Fig. 5b displays cracks at the metal-oxide interface

more commonly. After 200 days the oxidation kinetics indicates that Zircaloy-4 has gone through transition. Fig. 5c shows that the oxide is thicker and a layer of lateral cracks has formed. It must be noted that this is only a qualitative assessment of the SEM images, the question still remains as to whether the full network of lateral cracks occurs at transition, or during the subsequent accelerated oxidation as discussed in [13]. Quantitative image analysis of the defects is required to improve understanding of their relationship with the transition in the corrosion kinetics. One potential impact of these cracks is the destabilisation of the tetragonal phase, which should lead to further nano-scale crack and pore formation providing fast ingress routes for oxygen containing species [11,12].

3.3. Qualitative assessment of defects – ZIRLO™ & A-0%Sn

Figs. 6a–c and 7a–c show samples of ZIRLO™ and A-0%Sn material after 80, 140 and 160 days. These images were taken at 16,000× magnification and are designed to be representative examples of the oxide and oxide-metal interface. For the ZIRLO™ material the assessment of the images appears to show isolated cracks forming early on (80 days) but becoming more frequent and apparently interconnected at transition (140 days). After the rapid oxidation, associated with post-transition, it is clear that these cracks have formed a layer (160 days). This is similar to the behaviour seen for the Zircaloy-4 material. Assessing Fig. 1 the oxidation kinetics of the A-0%Sn material appear very similar to that of the ZIRLO™, with the exception that it does not go through transition after 140 days. Fig. 7a–c shows that although there are some small apparently isolated cracks they are significantly fewer in number than for the ZIRLO™ material. The A-0%Sn does not go
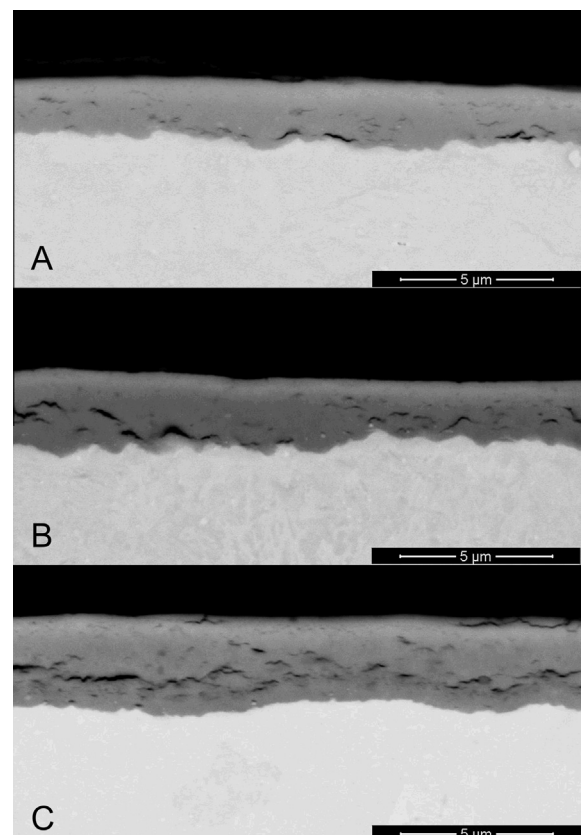

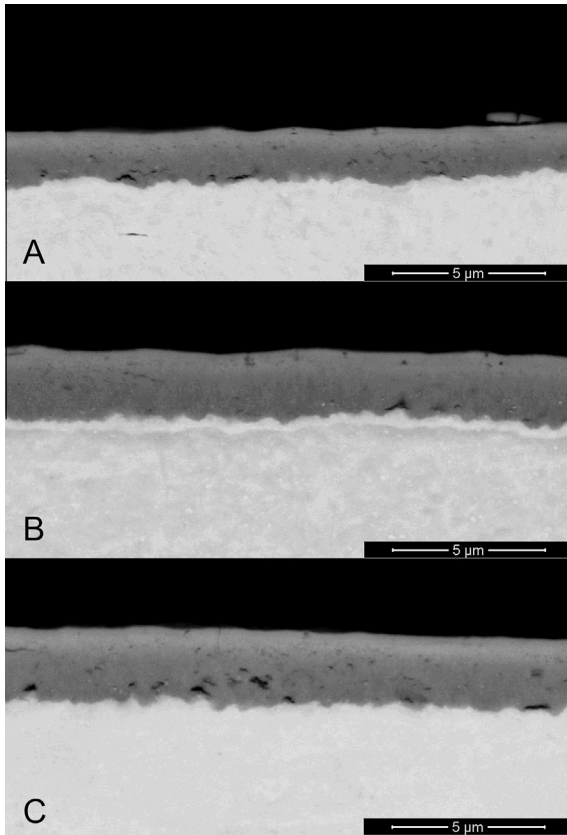**Fig. 6.** SEM cross section images (16000× mag.) of ZIRLO™ samples after 80 days, 140 days, and 160 days oxidation.

Fig. 7. SEM cross section images (16000× mag.) of A-0%Sn 80 days, 140 days and 160 days oxidation.
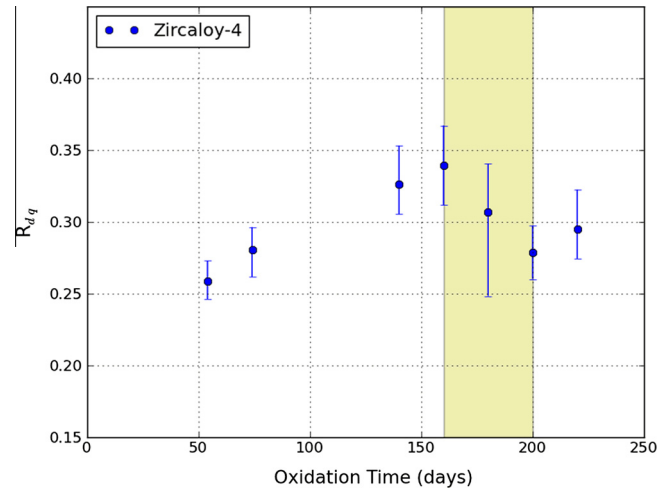

Fig. 8. Root mean square of the interface slope plotted against oxidation time for the Zircaloy-4 material. Each point represents the median of ~100 images, and the scatter bars represent the upper and lower quartiles.

through transition during the period analysed and no networks or layers of lateral cracks have been identified in any of the SEM images for this material. Although only a qualitative assessment, this indicates that removing the Sn from ZIRLO™ reduces the ability of the oxides to develop lateral cracks. Comparing these materials provides further evidence that the lateral cracks are in some way connected to transition and acceleration in the corrosion kinetics.

3.4. Interface roughness – Zircaloy-4

Parameters such as the root mean square (R_q) are based solely on the variation in amplitude along the interface, whereas parameters such as the Mean Spacing (RSM) are based solely on the spacing or wavelength of irregularities. R_{dq} is a hybrid parameter that measures the root mean square of the interface slope. In doing so this parameter takes into account changes in both the amplitude and the wavelength. Shown in Eq. (2), this is mathematically similar to the R_q parameter. The difference being that the slope of a given interval (Δ) has been substituted in for the height at a given interval (y). The result is a single value defining the interface roughness for each image taken.

$$R_{dq} = \sqrt{\frac{1}{N}\sum_{i=1}^{N}\Delta_i^2} \qquad (2)$$

Fig. 8 shows a plot comparing the interface roughness of Zircaloy-4 material with relation to oxidation time. Each data point is the median of ~100 images, with the scatter bars representing the upper and lower quartiles of the ranges. The yellow highlighted region represents the time frame in which transition is predicted to have occurred. Fig. 8 appears to show an increase in the R_{dq}

parameter up to 160 days, i.e. just before transition. As the material goes through transition there is a reduction in the interface roughness and it then seems to increase again.

The purpose of taking 100 images was to allow statistical analysis of the variation in interface roughness across a single sample. Fig. 9 show a series of histograms made for each of the Zircaloy-4 samples oxidised for different time periods. These distributions appear to have a single mode. After 180 days oxidation, i.e. during transition, the scatter bar shown in Fig. 8 is substantial. The distribution for this sample shown in Fig. 9 appears to demonstrate a bimodal distribution. The implication here is that some regions of the oxide have gone through transition whereas other regions have not. This is supported by the work presented in [25], which showed that the surface of the sample oxidised for ~180 days had a patchy appearance. It also suggests that there is local variation in the oxidation rate across any given sample, which further explains the level of scatter seen in the data across a single sample.

For the Zircaloy-4 material each SEM image can be used to define an average oxide thickness and the R_{dq} for that specific image. Fig. 10 shows the R_{dq} plotted against the oxide thickness for each image, totalling ~700 SEM images. It shows two distinct regions, there is an increase in R_{dq} from ~1.3 µm up to ~2.5 µm, after which it drops abruptly and then begins to increase again with increasing oxide thickness. Although there is some overlap, the separation in these regions is observed at 2.4 µm to 2.6 µm oxide thickness. Comparing with Fig. 4, this level of oxide thickness could be seen to correlate with immediately after transition, thereby relating the reduction in interface roughness with the rapid oxidation.

Comparing Figs. 8–10 indicates that for the Zircaloy-4 material there is an increase in interface roughness up to transition, followed by a sharp reduction relating to the rapid oxidation, and a subsequent increase as the oxide thickens. Parise et al. conducted finite element simulations indicating that the peaks in the interface roughness should be associated with localised out-of-plane tensile stresses that could be responsible for the formation of lateral cracks [18]. Qualitative assessment of the SEM images (e.g. Figs. 5–7) shows a clear trend towards the formation of lateral cracks above peaks in the interface roughness. This trend of isolated crack formation above interface roughness peaks has been observed previously in literature [13,21,22]. High resolution SIMS analysis has indicated that lateral cracks might impede oxygen diffusion directly below the crack [22]. However, as pointed out by
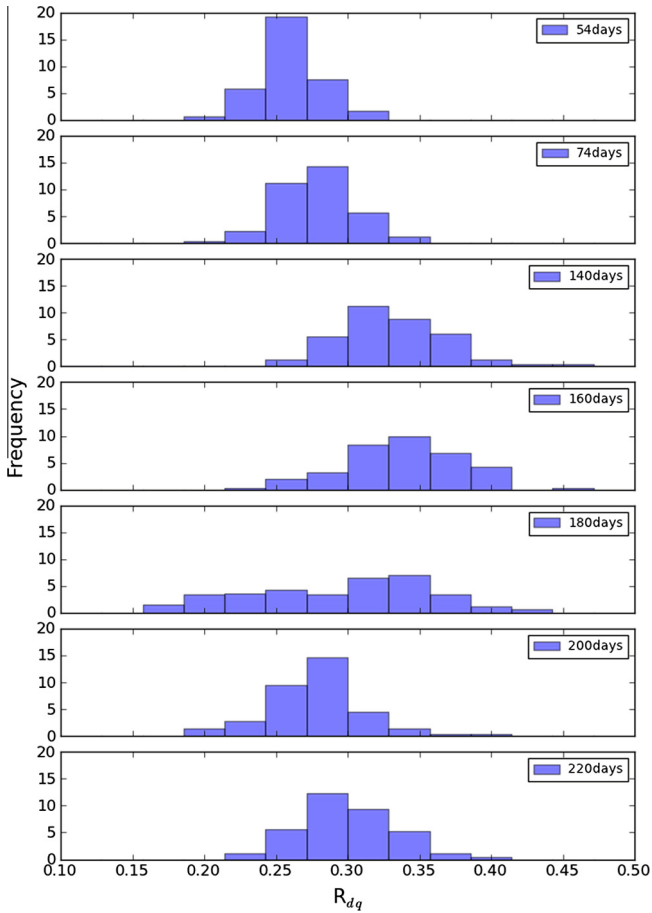
Fig. 9. Histograms of the R_{dq} for each set of $\sim$100 Zircaloy-4 cross-section images based on oxidation time.
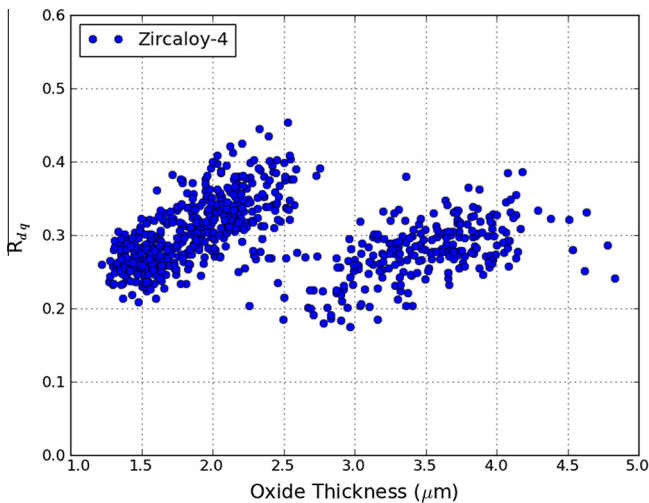

Fig. 10. The R_{dq} plotted against average oxide thickness for each individual cross section image of the Zircaloy-4 material.

Tejland et al. surface diffusion is much faster than grain boundary diffusion therefore increasing the number cracks in the oxide should increase the average oxygen diffusion rate [22]. Finite element analysis of the tetragonal to monoclinic phase transformation has shown that the formation and growth of lateral cracks should locally destabilise the tetragonal phase potentially leading to the formation of nano-scale cracks and pores [11]. This would create fast ingress routes for oxygen containing species.

3.5. Interface roughness – ZIRLO™ & A-0%Sn

Fig. 11 shows a plot comparing the interface roughness (R_{dq}) of ZIRLO™ and A-0%Sn materials with relation to oxidation time. Each data point is the median of only 30 images, with the scatter bars representing the upper and lower quartiles of the ranges. The green highlighted region represents the time frame in which transition is predicted to have occurred for the ZIRLO™ material. As with the Zircaloy-4, there appears to be an increase in the R_{dq} up to transition for the ZIRLO™. When compared with the Zircaloy-4, the oxidation time range over which the ZIRLO™ samples have been analysed is smaller. As one would expect, therefore, the change in the interface roughness is lower. However, the level of reduction in the R_{dq} after transition is similar to that shown for the Zircaloy-4 material.

The A-0%Sn material does not go through transition during the period analysed, and based on the work presented in [30] does not demonstrate acceleration in the oxidation kinetics after 280 days oxidation. This could potentially explain why any increase in the R_{dq} for the A-0%Sn material is very small. However, the magnitude of the R_{dq} is similar to that of the ZIRLO™ material, and yet comparing the SEM images qualitatively (examples shown in Figs. 6 and 7) indicated significantly fewer lateral cracks. Relating to the finite element analysis presented by Parise et al. [18], it raises the question of whether the interface roughness results in a lower stress concentration, or if the removal of Sn impacts the strength of the interface or oxide formed on A-0%Sn.

3.6. Stress & elastic energy – Zircaloy-4

Previously, synchrotron X-ray diffraction has been applied to oxides formed on the Zircaloy-4 material described earlier. Analysis included the tetragonal phase fraction, and the in-plane compressive stresses in both the monoclinic and tetragonal phases [4]. Using this data an average oxide stress can be calculated using Eq. (3).

$$\sigma_{avg} = (f_t \sigma_t) + (f_m \sigma_m) \tag{3}$$

where σ_{avg} is the average oxide stress, σ_t is the stress in the tetragonal phase, σ_m is the stress in the monoclinic phase, f_t is the tetragonal phase fraction and f_m is the monoclinic phase fraction. Fig. 12a shows this in-plane compressive stress plotted against oxidation time displaying a gradual reduction up to transition.
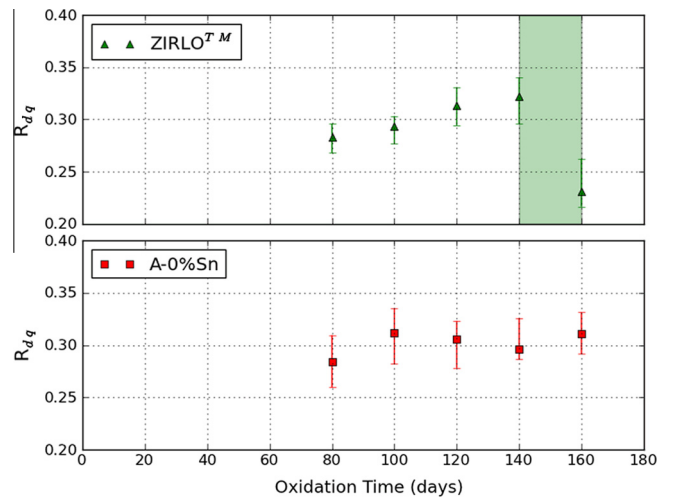

Fig. 11. Root mean square of the interface slope plotted against oxidation time for the ZIRLO™ and A-0%Sn materials. Each point represents the median of $\sim$100 images, and the scatter bars represent the upper and lower quartiles.

One potential mechanism for stress relaxation could be if the interfacial area is increasing due to localised plastic deformation [18]. In a similar way to the work presented in [23], the increase in interfacial length can be described as a strain, ε_I, by Eq. (3):

$$\varepsilon_I = \frac{(S - S_0)}{S_0} \tag{4}$$

where S is the interfacial length and S_0 is the initial interface length. It is impossible to know the initial surface roughness prior to oxidation for each of the areas imaged using SEM. As such the assumption is made that the interface was initially perfectly planar. Therefore, the width of each SEM image is used as the initial interface length. Fig. 13 shows the interface length change plotted against oxidation time. Each data point represents the median of 100 images and the scatter bars represent upper and lower quartiles. Although the pickling process used to prepare the samples should create a level interface it is noted that assuming a completely planar initial interface could potentially elevate these values by a small amount. However, as all samples had the same sample preparation, and all images have been treated the same, the differences between these points should be valid regardless of the initial interface length.

Previous work has indicated that this level of stress relaxation requires an in-plane strain in the order of ~0.5% [31,32]. Considering Fig. 13, ε_I changes by ~2% from 54 days to 160 days. Work by Tejland et al. has shown evidence of plastic deformation in the near surface metal which was attributed to the development of interface roughness [19]. Plastic deformation has also been predicted using finite element analysis in the work by Parise et al. [18] and Vermaak et al. [33]. This would indicate that at least some of the interface roughness development is due to a deformation mechanism attempting to relax stresses present at the metal-oxide interface. However, 2% strain is four times the level required to explain the stress relaxation observed using S-XRD. It could be possible that a mechanism other than oxidation growth stress is introducing more stress into the oxide layer, e.g. the expansion resulting from the tetragonal to monoclinic phase transformation [4,11]. Alternatively it could be that at least part of the increase in interface roughness results from localised variation in oxygen diffusion and preferential corrosion [17].

The development of interface roughness, and subsequent separation of the interface or fracture of the oxide, has been observed in a number of high temperature metal-oxide systems [16,17,23,24]. As with oxides formed on zirconium alloys, a common theme is the presence of a strong bi-axial compressive stress in the oxide layer.
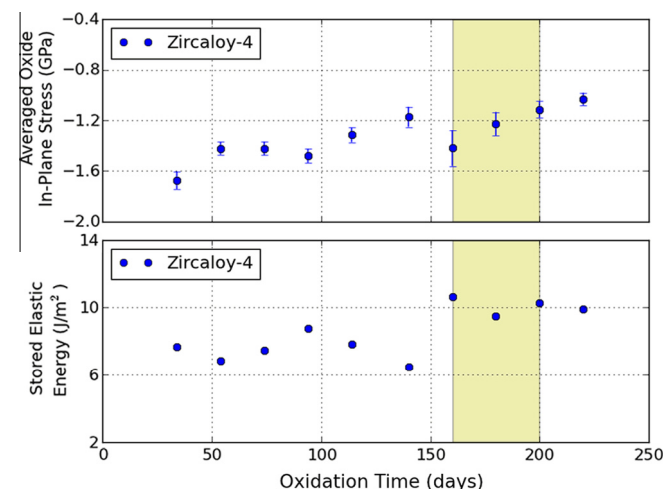

Fig. 12. Average in-plane stress and stored elastic energies for oxides formed on Zircaloy-4 based on S-XRD.
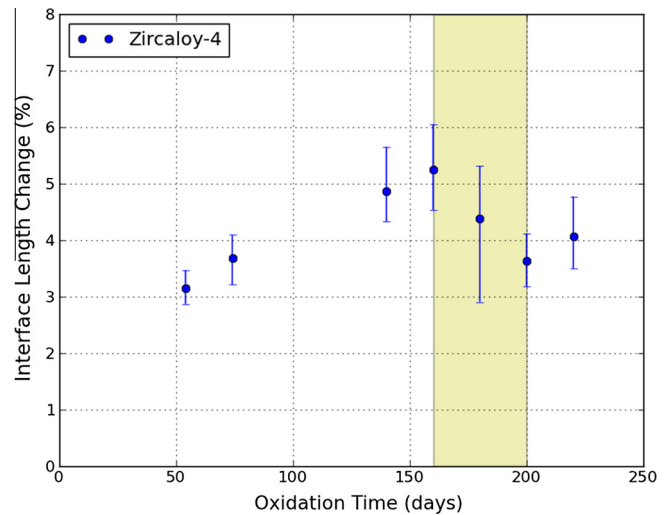

Fig. 13. Change in the interface length defined as a strain for Zircaloy-4 material.

Using basic fracture mechanics a common approach has been the application of an energy model. The in-plane compressive stress generates stored elastic energy in the oxide layer, which can be calculated using Eq. (5) [15,17].

$$U^* = \frac{(1 - v)h\sigma_{avg}^2}{E} \tag{5}$$

where U^* is the stored elastic energy, E is the elastic modulus for the oxide layer (253 GPa [30]), v is the Poisson's ratio (0.34 [30]) and h is the oxide thickness based on weight gain (Fig. 1). This stored elastic energy can be reduced by either; increasing the interfacial area and thereby reducing the constraint on the oxide, or by separation of the interface or fracture of the oxide layer [15]. Figs. 5 and 13 indicate that both mechanisms are occurring throughout the oxidation process, but that until transition fracture is only occurring locally. Fig. 12b shows the stored elastic energy for oxides formed on Zircaloy-4. Although there is some scatter in the results it appears to show a marked increase in the stored elastic energy immediately prior to transition. One hypothesis is that further increases in interfacial area are not sufficient to deal with this increase in stored elastic energy, or that strain hardening and increasing interfacial energy make increasing the interfacial area energetically unfavourable, and instead widespread fracture is energetically favourable.

3.7. Stress & elastic energy – ZIRLO™ & A-0%Sn

As with the Zircaloy-4 material, S-XRD has been used previously to analyse the stress levels in oxides formed on the ZIRLO™ and A-0%Sn tube material [30]. Using Eqs. (3) and (5) the average stress levels and stored elastic energies have been defined for the oxides formed on these materials and presented in Fig. 14. The green bar represents the estimate transition region of the ZIRLO™ material, and the red bar represents the estimated transition for the A-0%Sn material [30]. Linear trend lines have been fitted as the simplest way to help define some observed trends.

The first aspect to note is that the average oxide hoop stresses for oxides formed on the A-0%Sn tube are several hundred MPa lower than for oxides formed on ZIRLO™. The second aspect to note is that relaxation of the stresses is more prominent in the ZIRLO™ material. Fig. 15 shows the increase in interfacial length, ε_I, defined using Eq. (4). For the ZIRLO™ material up to transition, the increase in interfacial area presented in Fig. 15 appears to correlate with the
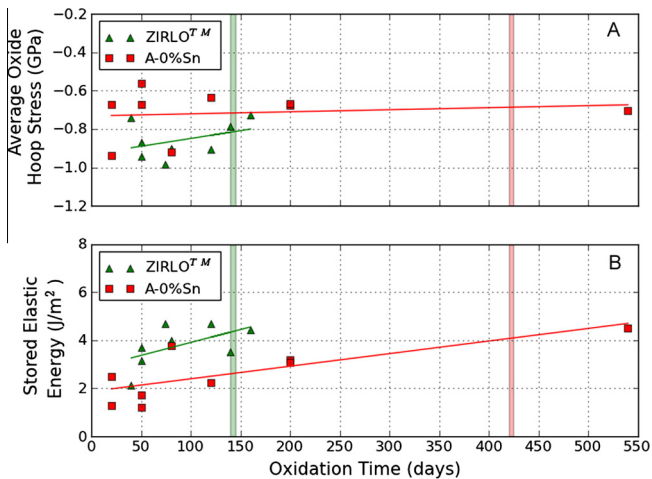
Fig. 14. Average in-plane stress and stored elastic energies for oxides formed on ZIRLO™ and A-0%Sn based on S-XRD.

reduction in hoop stress presented in Fig. 14. This is a similar trend to the behaviour observed in Zircaloy-4.

Interestingly for the A-0%Sn material, over the periods analysed, both the stress relaxation (Fig. 14) and changes in the interfacial area (Fig. 15) appear to be very small, if present at all. It is possible that the stress does not relax greatly, and the interface roughness does not change significantly, because the average hoop stress is significantly lower. Therefore, there is a reduced driving force. However, the magnitude of the interface roughness (Fig. 11) is comparable to that of the other materials, and S-XRD of thinner oxides shows some evidence of high compressive stresses (Fig. 14). Sn is known to increase the yield strength, hardening and creep resistance of zirconium alloys [34,35]. One possibility is that the interface roughness develops rapidly and relaxes the compressive stresses at a much earlier stage of oxidation. If the magnitude of the localised stresses above undulation peaks increases with the average stress level this could explain why a similar level of roughness produces fewer isolated lateral cracks in oxides formed on A-0%Sn when compared with oxides formed ZIRLO™.
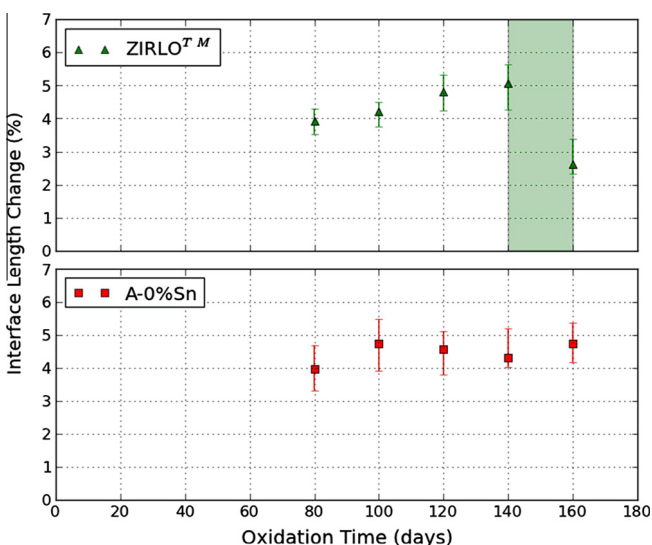
Fig. 14 compares the stored elastic energies of oxides formed on the ZIRLO™ and A-0%Sn materials over time. It can be seen that the stored elastic energy increases for both materials during oxidation. The level of the stored elastic energy is lower for the A-0%Sn material than for the ZIRLO™ material. Although the predicted transition point for the A-0%Sn is only an estimate [30], it seems that the level of the stored elastic energy at transition is approximately the same for oxides formed on both A-0%Sn and ZIRLO™.

4. Conclusions

This paper presents a detailed analysis of the development of roughness at the metal-oxide interface for samples of Zircaloy-4, ZIRLO™ and A-0%Sn. This has been achieved by mounting the samples in cross-section, imaging using SEM, extracting the interface using image analysis and detailed analysis of the interface profile. For the Zircaloy-4 material it was also possible to analyse the oxide thickness using SEM. Results indicated that SEM always predicts a thicker oxide layer to that predicted based on weight gain calculation.

Analysis of the interface roughness has been achieved primarily using the hybrid parameter R_{dq} (root mean square of the interface slope). Results indicated an increase in the interface roughness up to transition for both the Zircaloy-4 and ZIRLO™ materials. This is followed by a dramatic reduction associated with the period of accelerated oxidation after transition. The A-0%Sn material does not go through transition during the period analysed, and does not show a noticeable change in the interface roughness during the period analysed.

The interface profiles have also been analysed for changes in the interface length. This has then been correlated with previous synchrotron X-ray diffraction data to discuss increases in interfacial area relating to stress relaxation in oxide layer. S-XRD stress data can also be used to define the stored elastic energy in the oxide which has been related to interface roughness development, fracture of the oxide and transition in the oxidation kinetics. It appears that although the ZIRLO™ and A-0%Sn go through transition after different oxidation times, they should have the same level of stored elastic energy at transition because oxides formed on A-0%Sn exhibit a lower in-plane compressive stress.

Fig. 15. Change in the interface length defined as a strain for ZIRLO™ and A-0%Sn material.

References

[1] B. Cox, V. Kritsky, C. Lemaignan, V. Polley, I. Richtie, H. Ruhmann, V. Sishov, IAEA TECDOC 996 (1998).
[2] P. Bossis, F. Lefebvre, P. Barbéris, A. Galerie, Mater. Sci. Forum 369–372 (2001) 255.
[3] A. Yilmazbayhan, A. Motta, R.J. Comstock, G.P. Sabol, B. Lai, Z. Cai, J. Nucl. Mater. 324 (2004) 6.
[4] E. Polatidis, P. Frankel, J. Wei, M. Klaus, R.J. Comstock, A. Ambard, S. Lyon, R.A. Cottis, M. Preuss, J. Nucl. Mater. 432 (2013) 102.
[5] A. Ly, A. Ambard, M. Blat-Yrieix, L. Legras, P. Frankel, M. Preuss, C. Curfs, G. Parry, Y. Brechet, in: Zircon. Nucl. Ind. 16th Int. Symp. ASTM STP 1529, 2011, pp. 682–707.

[6] N. Ni, Study of Oxidation Mechanisms of Zirconium Alloys by Electron Microscopy, University of Oxford, 2011.

[7] M. Preuss, P. Frankel, S. Lozano-Perez, D. Hudson, E. Polatidis, N. Ni, J. Wei, C. English, S. Storer, K.B. Chong, M. Fitzpatrick, P. Wang, J. Smith, C. Grovenor, G. Smith, J. Sykes, B. Cottis, S. Lyon, L. Hallstadius, R.J. Comstock, A. Ambard, M. Blat-Yrieix, in: Zircon. Nucl. Ind. 16th Int. Symp. ASTM STP 1529, 2011, pp. 649–681.

[8] N. Ni, D. Hudson, J. Wei, P. Wang, S. Lozano-Perez, G.D.W. Smith, J.M. Sykes, S.S. Yardley, K.L. Moore, S. Lyon, R. Cottis, M. Preuss, C.R.M. Grovenor, Acta Mater. 60 (2012) 7132.

[9] N. Ni, S. Lozano-Perez, M.L. Jenkins, C. English, G.D.W. Smith, J.M. Sykes, C.R.M. Grovenor, Scr. Mater. 62 (2010) 564.

[10] N. Petigny, J. Nucl. Mater. 280 (2000) 318.

[11] P. Platt, P. Frankel, M. Gass, R. Howells, M. Preuss, J. Nucl. Mater. 454 (2014) 290.

[12] J. Chevalier, L. Gremillard, A.V. Virkar, D.R. Clarke, J. Am. Ceram. Soc. 92 (2009) 1901.

[13] N. Ni, S. Lozano-Perez, J.M. Sykes, G.D.W. Smith, C.R.M. Grovenor, Corros. Sci. 53 (2011) 4073.

[14] P. Bossis, G. Lelievre, in: Zircon. Nucl. Ind. 12th Int. Symp. ASTM STP 1354, Astm Intl, 2000, pp. 918–945.

[15] Z. Suo, J. Mech. Phys. Solids (1995).

[16] R. Christensen, D. Lipkin, D. Clarke, Acta Mater. 44 (1996) 3813.

[17] H. Evans, Int. Mater. Rev. 40 (1995).

[18] M. Parise, O. Sicardy, G. Cailletaud, J. Nucl. Mater. 256 (1998) 35.

[19] P. Tejland, H.-O. Andrén, J. Nucl. Mater. 444 (2014) 30.

[20] A. Saillard, M. Cherkaoui, H. El Kadiri, Model. Simul. Mater. Sci. Eng. 19 (2011) 015009.

[21] S.S. Yardley, K.L. Moore, N. Ni, J.F. Wei, S. Lyon, M. Preuss, S. Lozano-Perez, C.R.M. Grovenor, J. Nucl. Mater. 443 (2013) 436.

[22] P. Tejland, H.-O. Andrén, J. Nucl. Mater. 430 (2012) 64.

[23] V.K. Tolpygo, D.R. Clarke, Acta Mater. 46 (1998) 5153.

[24] X. Gong, D. Clarke, Oxid. Met. 50 (1998).

[25] J. Wei, P. Frankel, M. Blat, A. Ambard, R.J. Comstock, L. Hallstadius, S. Lyon, R.A. Cottis, M. Preuss, Corros. Eng. Sci. Technol. 47 (2012) 516.

[26] J. Lin, H. Li, J.A. Szpunar, R. Bordoni, A.M. Olmedo, M. Villegas, A.J.G. Maroto, Mater. Sci. Eng. A 381 (2004) 104.

[27] D. Hudson, A. Cerezo, G.D.W. Smith, Ultramicroscopy 109 (2009) 667.

[28] M. Steinbrück, Oxid. Met. 70 (2008) 317.

[29] D. Douglass, Oxid. Met. 1 (1969) 127.

[30] J. Wei, P. Frankel, E. Polatidis, M. Blat, A. Ambard, R.J. Comstock, L. Hallstadius, D. Hudson, G.D.W. Smith, C.R.M. Grovenor, M. Klaus, R.A. Cottis, S. Lyon, M. Preuss, Acta Mater. 61 (2013) 4200.

[31] P. Platt, P. Frankel, M. Preuss, M. Gass, M. Bamber, I. Symington, R. Howells, in: Proc. TopFuel, Manchester, 2012, pp. 17–21.

[32] P. Platt, E. Polatidis, P. Frankel, M. Klaus, M. Gass, R. Howells, M. Preuss, J. Nucl. Mater. 456 (2015) 415.

[33] N. Vermaak, G. Parry, R. Estevez, Y. Bréchet, Acta Mater. 61 (2013) 4374.

[34] C. Nam, K. Kim, M. Lee, Y. Jeong, J. Korean Nucl. Soc. 32 (2000) 372.

[35] S.L. Wadekar, S. Banerjee, V.V. Raman, M.K. Asundi, in: Zircon. Nucl. Ind. 9th Int. Symp. ASTM STP 1132, 1991, pp. 140–155.